Available online at www.sciencedirect.com
ScienceDirect
Mathematics and Computers in Simulation 202 (2022) 316–330
MATHEMATICS AND COMPUTERS IN SIMULATION
www.elsevier.com/locate/matcom

Original articles

Diagnosis of breast cancer for modern mammography using artificial intelligence

R. Karthiga, K. Narasimhan*, Rengarajan Amirtharajan

School of Electrical & Electronics Engineering, SASTRA Deemed University, Thanjavur 613 401, India

Received 20 December 2021; accepted 30 May 2022
Available online 6 June 2022

Abstract

The diagnosis of breast cancer, one of the most common types of cancer worldwide, is still a challenging task. Localisation of the breast mass and accurate classification is crucial in detecting breast cancer at an early stage. In machine learning-based classification models, performance is dependent on the accuracy of extracted features and is susceptible to saturation problems. Deep learning methods are currently used to learn self-regulating top-level features and achieve remarkable accuracy. It has long been recognised that mammography is competent for the early detection of cancer cells. Thus the technique of image segmentation and artificial intelligence can be applied to the initial stage diagnosis of breast cancer. The proposed method is composed of two major approaches. In the first, the transfer learning method is employed. In the second, convolution neural network architecture is constructed, and its hyper-parameters are adjusted to achieve accurate classification. The result indicates that the proposed methods achieve significant accuracy for MIAS (95.95%), DDSM (99.39%), INbreast (96.53%), and combined datasets (92.27%). Comparison of results of the proposed approach with current schemes demonstrates its efficiency.

Keywords: Breast cancer; Mammogram; Convolutional neural network; Polynomial curve fitting

1. Introduction

Breast cancer is the most common cancer rate among women worldwide, and it is the second leading cause of death, according to the World Health Organisation (WHO) annual global cancer report 2018 [1]. Nevertheless, early diagnosis of cancer helps prevent the death rate from cancer. The screening examination is the first step in identifying breast cancer. Mammography has long been considered the most effective and least expensive way to diagnose breast cancer [2]. Recently, Breast Cancer has been diagnosed using Computer-Assisted Diagnosis (CAD) [3]. However, traditional methods are limited in accuracy and processing time [4].

Breast cancer cases are predicted to reach 2, 68, 600, and 2670 states identified men with breast cancer in 2019. It is possible to improve the survival rate of most cancer patients by early diagnosis and proper treatment [5]. Typically, breast cancer is treated by surgery, radiation, chemotherapy, and hormonal therapy. A breast cancer diagnosis can be taken through different imaging techniques such as mammography, magnetic resonance imaging (MRI), ultrasound, or histopathology. In this case, mammography is the most efficient way to determine whether an abnormality exists in a breast [6]. Various studies have estimated that mammography reduces the risk of death by 30% to 70% [7].

* Corresponding author.
E-mail address: knr@ece.sastra.edu (K. Narasimhan).

https://doi.org/10.1016/j.matcom.2022.05.038

Diagnostic inaccuracy in breast cancer is caused by low-quality imaging and physician oversight, which lead to misreadings. Additionally, 52% of errors are the result of misinterpretation. As a result of Computer-Aided Diagnosis (CAD) systems, breast cancer can often be detected at the earliest stages, overcoming the difficulties associated with mammography. With CAD systems, diagnostic images are combined with computer systems via different image processing techniques such as pattern recognition and artificial intelligence using convolutional neural networks (CNN) [8]. Radiologists can use the CAD system to reduce their workloads and minimise the risk of breast cancer while also increasing the accuracy of diagnosis.

Based on a study by Brem et al. CAD can improve the physicians' diagnostic sensitivity by 21.2% and help them make a more accurate diagnosis [9]. In [8], the authors utilised 70% data for testing, and the remaining data is used to perform validation. As a result, they achieved 97.30% accuracy rates by using SVM classifiers. Several techniques have been developed in the past few years to improve the accuracy of current CAD systems using preprocessing techniques, such as segmentation, hand-crafted feature extraction, and deep learning. In contrast, hand-crafted features affect accuracy significantly, whereas deep learning can automatically improve accuracy by analysing the data.

In this study, deep learning models are used to improve breast cancer classification accuracy. We explored several preprocessing methods to enhance the image, including CLAHE, cropping, augmentation, and polynomial curve fitting for segmentation. The significant features are extracted from the preprocessed image using CNN techniques and classified into benign and malignant masses. Moreover, pre-trained models (AlexNet, VGG16 and VGG19) have also been evaluated to improve results. The results show that VGG-19 achieved better results for all three datasets. The significant contributions of the proposed method are:

- This paper studies and improves the deep network architecture also increases the diagnostic accuracy of breast lesions from digital X-ray mammogram
- The three mammogram databases are utilised in this proposed work
- Through preprocessing, the quality and quantity can be increased, which makes the rate of accuracy is more
- The CNN classifier achieved promising diagnosis performance with an accuracy of 95.95% for MIAS, 99.39% for DDSM, 96.53% for INbreast, and 92.27% for combined datasets
- The results outperform the methods that are taken for comparison

This article has been organised as follows. Section 2 focuses on various preprocessing techniques used in the classification of breast cancer utilising deep learning. Section 3 presents a detailed analysis of the proposed algorithm that uses CNN architecture and can be applied to MIAS, DDSM, and IN breast datasets. In Section 4, results and methods are summarised, reviewed, and compared with state-of-the-art performance. Finally, Section 5 concludes the paper with its significant findings.

2. Related works

The research community has recently proposed several CAD systems for determining and categorising breast masses. The methods employed to develop these CAD systems can be divided into two phases: the first stage involves preprocessing, including image enhancement, augmentation, segmentation, and cropping. Methods for preprocessing are completely based on conventional machine learning techniques. In the second phase, implementation uproots the features of mammography using Convolutional Neural Networks (CNNs).

Shen et al. [10] designed a CAD system based on discrete wavelet transformations and Gray Level Co-occurrence Matrixes (GLCMs) for features extraction. This classification is accomplished by analysing Deep Belief Networks (DBN). This assessment shows 91.5% accuracy based on MIAS data. Debelle et al. [11] used Bethezata General Hospital (BGH) and Mammographic Image Analysis Society (MIAS) datasets to classify breast cancer. This paper extracts and evaluates GLCM and Gabor features with five classifiers (SVM, KNN, MLP, RF, and NB) and Inception-V3. Based on the results of this feature fusion, the accuracy results reached 99% (BGH) and 97.46% (MIAS).

According to [12], the authors designed a kernel extreme learning machine (KELM) for predicting the outcome of mammograms by using a wrapper-based system. It was demonstrated in the practical application of this approach that 97.9% accuracy was achieved with MIAS and 92.61% accuracy with DDSM. In [13], the author's employed multi-class support vector machine (MSVM) and K-means clustering as the preprocessing methods for feature

extraction. They achieved 96.9% (SVM), 93.8% (KNN), 89.7% (LDA) and 88.7% (Decision tree) respectively. In [14], the author proposed a deep convolutional neural network for identifying benign and malignant tumours using mini-MIAS and BCDR (Breast Cancer Digital Repository). In the end, they achieved results of 87% (MIAS mass), 98% (MIAS training accuracy), 88% (BCDR mass) and CNN — 98% (BCDR training accuracy).

Rabidas et al. [15] stipulated that global similarity and uniform local binary patterns were described to classify lesions as benign or malignant. A stepwise logistic regression approach was used for Fisher Linear Discriminant Analysis (FLDA) to select the most appropriate set of features. The AUC of 0.98 was achieved using the MIAS database with a classification accuracy of 94.57%. Furthermore, they achieved 85.42% classification accuracy with a 0.93 AUC for the DDSM database. Yoon et al. [16] used the morphological method and the random sample consensus (RANSAC) algorithm and achieved 92.2% accuracy.

Two-dimensional discrete wavelet transform (2D-DWT), discrete curvelet transform (DCT), and convolutional neural network (CNN) are utilised by Jadoon et al. [17] for the classification of normal, benign, and malignant masses. This proposed strategy achieved an accuracy of 81.83% (CNN-DW) and 83.74% (CNN-CT). Saleem et al. [18] used an augmented dataset developed by MIAS and achieved 92.1% classification accuracy.

Zeiser et al. [19] implemented U-net models for the DDSM dataset and acquired 85.95% classification accuracy. In [20], the authors reached an AUC of 0.99 and 96% overall sensitivity results by utilising multiscale CNN architecture. Finally, Zhang et al. [21] introduced a novel algorithm for breast cancer classification. The identity of cancer cells is achieved through fusion criteria in CNN using mini-MIAS, CBIS-DDSM, and INbreast datasets combined. They obtained an AUC of 0.97 and classification accuracy of 94.3%.

In [22], the authors used a combination of k-mean clustering, RNNs, CNNs, random forests, and boosting techniques to improve accuracy. The authors achieved significant accuracy with MIAS (95% accuracy) and DDSM (96% accuracy). A group of researchers investigated fusion models using transfer learning models using VGG-16 and VGG-19 [23] and reached 0.8906 for model 1 and 0.875 for model 2.

Dhungel et al. [24] utilised the deep learning and random forest technique to diagnose benign and malignant masses. The authors used active contour modelling for preprocessing and achieved a classification accuracy of 0.91 and an AUC of 0.87. By utilising INbreast datasets, Ribli et al. [25] framed a fast R-CNN that classified breast lesions with an AUC of 0.87. In [26], the authors used MIAS, DDSM and INbreast datasets and accomplished satisfactory results. The test accuracy results are 93.39% (MIAS), 91.2% (DDSM), 93.04% (INbreast), and 90.17% (MIAS+DDSM+INbreast). In comparison to current state-of-the-art methods, our approach yields superior results

3. Proposed methodology

Here we briefly summarise data collected in this section, including MIAS, DDSM, and IN breast. The entire development process of the proposed CAD system began with the preprocessing phase and the building of CNNs. This preprocessing stage includes CLAHE, data augmentation, segmentation using polynomial curve fitting, and cropping the breast region. In CNN, preprocessed images can classify benign and malignant tumours. By comparing the results, it is evident that CNN has a higher accuracy level than transfer learning models. Therefore, this scheme can be considered an impressive tool that helps radiologists accurately determine true positives and false negatives. The proposed scheme is envisioned in Fig. 1.

3.1. Datasets

A CAD system has been proposed by using the three standard mammography datasets. The three datasets are the Mammogram Image Analysis Society (MIAS) [27] dataset, the Digital Dataset for Screening Mammography (DDSM) [28], and the INbreast dataset [29]. The MIAS dataset comprises 322 images in Portable Gray Map (PGM) format. The dataset contains 207 normal, 63 benign, and 52 malignant cases. The size of the image is 1024×1024. The DICOM-formatted DDSM images contain images of mass cases, calcification cases, and ROI images. A total of 410 breast lesions from 115 cases are included in the INbreast dataset. The dataset contains 41 benign images from 18 cases and 75 malignant images from 32 cases in DICOM format.

The datasets are sourced from the Mendeley repository [30], which comprises MIAS, DDSM, INbreast, and the integration of these three datasets. A dataset collection contains benign and malignant masses resized to 227×227 pixels and stored in Portable Network Graphics (PNG) format. Among the datasets in the repository are 53 lesions from the MIAS repository, 2188 lesions from the DDSM repository, and 106 lesions from INbreast.

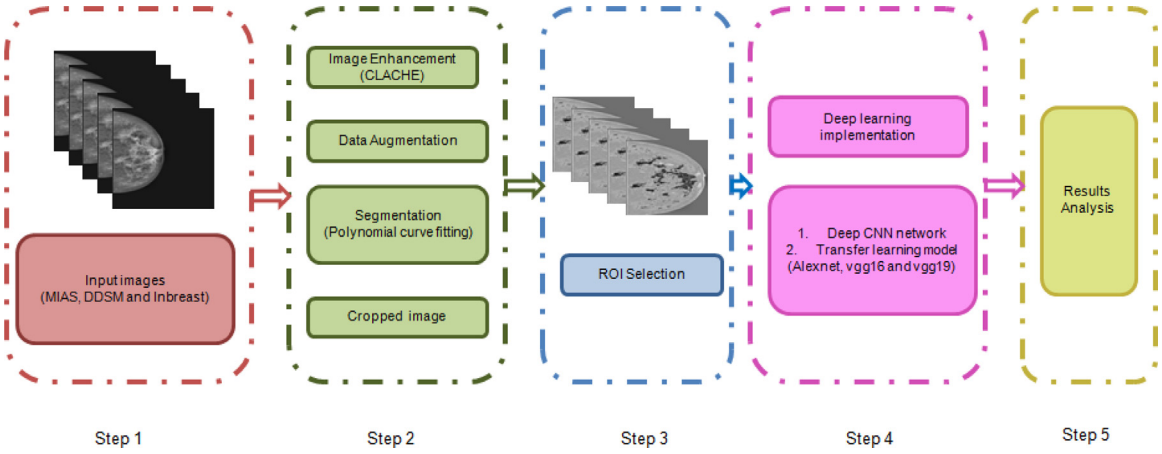

Fig. 1. Schematic representation of the proposed scheme.

Table 1
Dataset specifications.

Datasets	Number of images
MIAS	3816
DDSM	13128
INbreast	7632
Integrated datasets (MIAS+DDSM+INbreast)	24576

These datasets are compiled from preprocessed two-phase imagery combined with CLAHE and data augmentation. The datasets are compiled from two-phase images combining CLAHE and augmentation. To accomplish the proposed CAD, the whole augmented image set is used. A list of the augmented datasets is presented in Table 1.

3.2. Pre-processing

By using preprocessing, a series of modifications can be used to enhance the performance of a classification system. This step is intended to eliminate image noise and unwanted portions of the background from input images. In addition, artifacts such as medical labels and a broad black area in the original mammogram data can influence the accuracy results of the CAD system [31]. Therefore, the preprocessing step is utilised to remove unwanted artifacts from mammogram images. A segmentation process followed by image enhancement was used to improve results. Specifically, the preprocessing concerns two actions: enhanced images and cropped segmentation.

3.2.1. Augmented image enhancement

In this case, the given dataset image is preprocessed through two stages: Contrast Limited Adaptive Histogram Equalisation (CLAHE) and data enhancement. The CLAHE algorithm segments the images into non-overlapping blocks and clips each block according to a predefined coefficient on the scale [32]. Afterwards, histogram bins are used to redistribute the blocks. To achieve effective classification, a convolution neural network (CNN) requires a great deal of data. Once the CLAHE enhanced image is converted, several rotations, flipping, and other operations are applied to the dataset to enhance it.

3.2.2. Cropped segmentation

The segmentation process involves partitioning the input image into multiple regions that are easy to isolate and analyse. The segmentation locates the object and the boundaries in the image. This article utilises higher-order polynomial distributions to fit the polynomial curve [32,33]. The curve fitting process determines the appropriate fitting, and the mathematical equation is used to locate the data points. The higher-order polynomial equation is

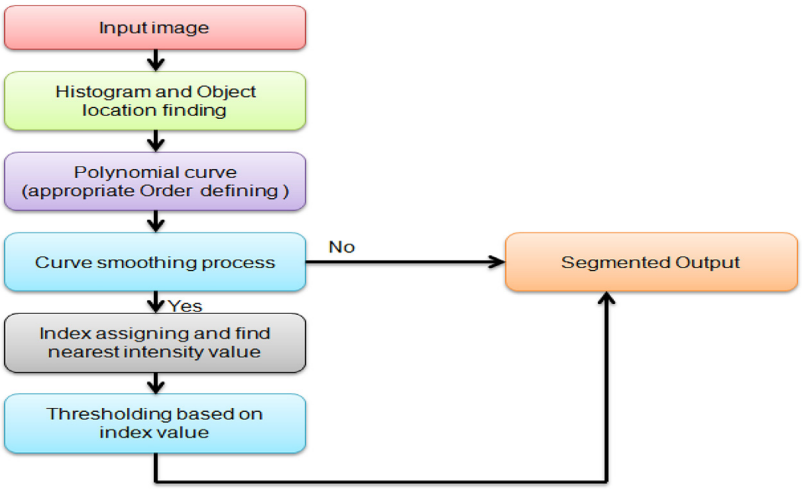

Fig. 2. Representation of polynomial curve fitting segmentation process.

derived from various polynomial equations. Fig. 2 highlights the process of segmentation. To apply the polynomial curve fitting, it is necessary to calculate the image's histogram to locate the target. A polynomial equation p(x) is defined as a polynomial with degree n involving a matrix (x). The data are fitted from p(x(i)) to p(y(i)):

$$p(x) = p_1 x^n + p_1 x^{n-1} + \cdots + p_n x + p_{n+1} \tag{1}$$

The fitting of the curve can be performed residue over the input image, and the higher-order polynomial values can be adjusted once the best fit has been identified. Through the use of intensity values, the segmentation is done based on different indexes. For this calculation, Eq. (2) reveals the threshold value. The closest match to the nearest mean dataset value is determined by comparing the value to the nearest value in the dataset. A polynomial function was used to obtain finer segmentation results, regardless of the data input type.

$$Threshold = \frac{\sum_{k=1}^{h} \sum_{l=1}^{w} X(k,l)}{h \times w} \tag{2}$$

Where $X(k,l)$ defined as datasets, h and w are the height and the width of the given input image.

The region of interest (ROI) plays a vital role in removing labels in mammogram images. The two diagonal points (Xmin, Ymin) and (Xmax, Ymax) cover the entire mass and create the bounding box that contains ROI. The bounding box of the mammogram image is cropped out, and the resulting images are shown in Fig. 3.

3.3. Convolution neural network experimental design

Based on human perception with machine learning, the features are in accurate compared to CNN [34]. Machine learning advances may allow CAD for mammography to become more valuable in clinical practice with the help of Artificial Intelligence using deep neural networks [35]. Tumour selectivity imaging and other biology techniques will inevitably converge in the age of artificial intelligence, resulting in notable advances in the treatment and diagnosis of cancer [36]. Artificial intelligence in breast imaging, including mammography, ultrasound, and magnetic resonance imaging, has been studied in different clinical scenarios. By combining AI tools with breast imaging software, images can be interpreted clinically for better results and more innovative approaches to patient care can be taken. This study examines the current state of knowledge and potential applications of artificial intelligence-enhanced breast imaging in clinical practice [37].

The convolution neural network (CNN), a popular deep learning technique, is used for classification regression and object recognition [38]. This section provides an overview of the design of CNN layers and mass detection using CAD. The CNN is comprised of layers based on biologically oriented models to shift information from the bottom up [39]. In deep learning, superior results have been achieved in comparison to traditional hand-crafted methods. Furthermore, the large number of parameters in CNN allows each layer to achieve extraordinary results [40].

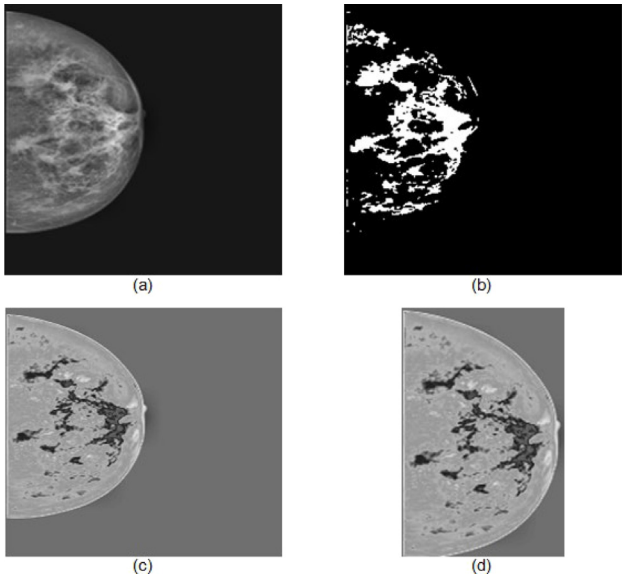

Fig. 3. (a) Original input image (b) Black and white conversion (c) Segmented image (d) Cropped image.

In mammogram images, preprocessed images contain features that CNN can extract to describe the tumour. In the first convolution layer, the edges and simplest textures are identified. Layers beneath the surface reveal textures and patterns that are more complicated. This last convolution layer identifies the details of each object in the input image. In the pooling process, a non-linear down-sampling is performed after convolution. Pooling layers allows the dimension on intermediate feature maps to be reduced to enhance robustness.

CNN utilises the fully connected layer to categorise based on the features. The kernel is a filter in the form of a small square that relates two pixels. Then, a neuron simulation is performed using an elementwise non-linear operator called the activation function. For deep learning, various activations are used, such as tanh, stochastic gradient descent (SGDM) and rectified linear units (ReLU).

In this work, the results of comparisons were made with different activation layers and are tabulated in Table 2. In addition, the feature maps will be spatially positioned in the normalisation layer, which will help enhance the representation of the input data. The proposed CNN architecture can classify benign and malignant masses accurately. It comprises three convolution layers, two max-pooling layers, five ReLU layers, three batch normalisation layers, and three fully-connected layers. The proposed architecture can be seen in Fig. 4. With this architecture, layers with a stride of two are utilised for maximum pooling.

Each convolution layer utilises stride, 1, and padding together to extract the features. Then, the fully connected layers 512, 128 and 2 are activated via the ReLU function. Finally, the output layer identifies the prediction's class based on features learned from the softmax layer.

Specifically, the proposed work focused on reducing the number of layers, reducing the number of parameters for training, and strengthening the feature transmission. An experiment is initially carried out with finely tuned numbers of layers. Then, we have further increased the layers to increase accuracy. Consequently, the accuracy decreases with further increments. Therefore, the final increasing accuracy architecture is fixed with the proposed architecture. The layer analysis summarised in Table 2 explains the proposed model. The ReLU activation method is used for layers that are hidden. A Relu activation function gives a zero result if the input is less than zero; otherwise, it returns the same result as the input. According to Eq. (3), the activation function of ReLU is as follows:

$$f(x) = \max(x, 0) \tag{3}$$

The classification layer comes after the fully connected layer, which specifies whether the results are benign or malignant.

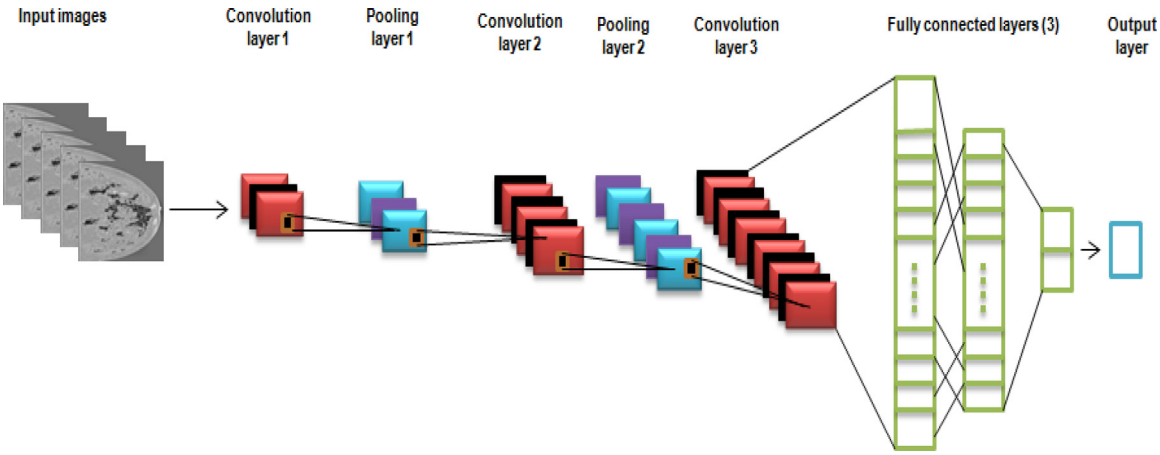

Fig. 4. Representation of the proposed CNN layers.

3.4. Deep convolution neural network pre-trained models

Many inspiring and impressive deep learning algorithms have been developed in recent years, extending their layers with deeper and deeper layers. Typically, state-of-the-art networks are composed of layers from 7 to 1000 layers. Here, we analysed the classification performance of CNN with that of the different pre-trained networks Alexnet, VGG-16, and VGG-19.

Kirzhevsky et al. [41] launched ImageNet ILSVRC in 2012 with a deep network and managed a 15.3% error rate on their test. Twenty-six percent of the second test results were incorrect. A typical Alexnet consists of five convolution layers, three max-pooling layers, and two fully connected layers. This proposal performs significantly better than existing benchmark tasks with innovative methods.

Research from Oxford University developed diverse versions of the pre-trained deep CNN. The VGG-16 network is regarded as one of the best and simplest networks. This network focuses on the alternation between the convolution and dropout layers. The 3×3 kernels are utilised in this network, which results in larger fields in the respective areas.

Network layers consist of thirteen convolutional layers, five pooling layers, and a fully connected layer. According to ImageNet's test results, this network results in an error rate of 9.9%. In [42], the authors implemented a 19-layer CNN architecture and obtained the best results in the localisation of ImageNet. Furthermore, the VGG-19 kernel size is 3×3, significantly improving the results.

This study uses pre-trained deep convolutional neural network models Alexnet, VGG-16, and VGG-19 and proposes improved networks to compare the results. In practice, the network training is conducted after fine-tuning and optimising the model's parameters. Normally, the parameters in pre-trained models are concentrated in layers of fully connected parameters. Multi-class classifications are intended to be classified by original networks. The article discusses the binary classification of cancer (Benign and Malignant). As a result, the fully connected layers are replaced with two new fully connected layers. These improved pre-trained models comprise convolution layers, max-pooling layers, fully connected layers, and softmax layers. The fine-tuned framework is illustrated in Fig. 5.

4. Experimental results and discussions

The CNN was implemented using the MATLAB 2018b version on an Intel i5 processor. This proposed model has an input size of 227×227. The model is run separately and then combined with three datasets (MIAS, DDSM, INbreast). Analysing the accuracy and time stamps of the proposed model with different architectures is a crucial part of its evaluation. Then the CNN architecture is compared with pre-trained models Alexnet, VGG-16 and VGG-19.

The performance of the system is measured using 24,576 mammographic augmented images. Mendeley contains datasets for MIAS, DDSM, and INbreast, curated from the Mendeley repository. During classification, the mammographic input has been divided into two phases (training and validation phases). Of the total 24,576 images,

Table 2
Network analysis using proposed CNN.

Layers	Name	Layers	Image Size	Learnable Parameters	Total Learnable parameters
1	Image input (227 × 227 × 1 images with 'zerocenter' and normalisation)	Input Layer	227 × 227 × 1	–	–
2	conv(1) ('8' - 3 × 3 × 1 convolution with stride '1' value and padding 'same')	Convolution Layer	227 × 227 × 8	(3 × 3 × 1 × 8)-Weights (1 × 1 × 8)-Bias	80
3	batchnorm(1) (Batch normalisation — 8 channels)	Batch Normalisation Layer	227 × 227 × 8	(1 × 1 × 8)-Offset (1 × 1 × 8)-Scale	16
4	relu(1) (ReLU)	ReLU Layer	227 × 227 × 8	–	–
5	maxpool(1) (2 × 2 max pooling with stride '2' and padding [0 0 0 0])	Max pooling Layer	113 × 113 × 8	–	–
6	conv(2) ('6' - 3 × 3 × 8 convolution with stride '1' and padding 'same')	Convolution Layer	113 × 113 × 16	(3 × 3 × 1 × 16)-Weights (1 × 1 × 16)-Bias	1168
7	batchnorm(2) (Batch normalisation 16 channels)	Batch Normalisation Layer	113 × 113 × 16	(1 × 1 × 16)-Offset (1 × 1 × 16)-Scale	32
8	relu(2) (ReLU)	ReLU Layer	113 × 113 × 16	–	–
9	maxpool(2) (2 × 2 max pooling with stride '2' and padding [0 0 0 0])	Max pooling Layer	56 × 56 × 16	–	–
10	conv(3) ('32' - 3 × 3 × 8 convolution with stride '1' and padding 'same')	Convolution Layer	56 × 56 × 32	(3 × 3 × 1 × 32)-Weights (1 × 1 × 32)-Bias	4640
11	batchnorm(3) (Batch normalisation — 32 channels)	Batch Normalisation Layer	56 × 56 × 32	(1 × 1 × 32)-Offset (1 × 1 × 32)-Scale	64
12	relu(3) (ReLU)	ReLU Layer	56 × 56 × 32	–	–
13	fc(1) (512 fully connected layer)	Fully connected Layer	1 × 1 × 512	(512 × 100352)-Weights (512 × 1)-Bias	–
14	relu(4) (ReLU)	ReLU Layer	1 × 1 × 512	–	–
15	fc(2) (128 fully connected layer)	Fully connected	1 × 1 × 128	(128 × 512)-Weights (128 × 1)-Bias	65664
16	relu(5) (ReLU)	ReLU Layer	1 × 1 × 128	–	–

(*continued on next page*)

80% are utilised for training, and 20% are used for validation. According to Table 3, the results of analysing the proposed CNN with different optimisation methods are listed. Based on the accuracy analysis, the RMSprop optimiser achieves benchmark results compared to other optimisers.

Table 2 (*continued*).

Layers	Name	Layers	Image Size	Learnable Parameters	Total Learnable parameters
17	fc(3) (2 fully connected layer)	Fully connected Layer	1 × 1 × 2	(2 × 128)-Weights (2 × 1)-Bias	258
18	softmax (softmax)	Softmax Layer	1 × 1 × 2	–	–
19	classoutput (crossentropy with benign masses and malignant masses)	Classification output	–	–	–

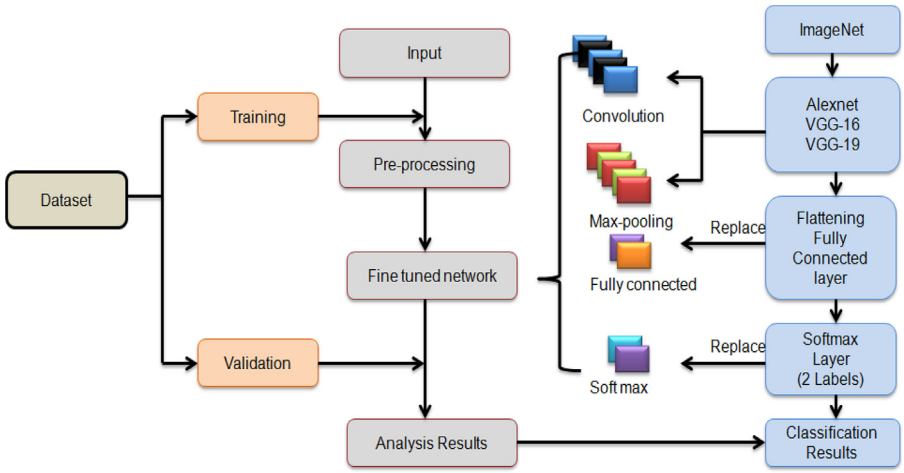

Fig. 5. Schematic representation of modified pre-trained models.

Table 3
Comparison analysis using various optimisers.

Optimisers	MIAS (%)	DDSM (%)	INbreast (%)	MIAS+DDSM+ INBREAST (%)
SGDM	94.39	97.43	94.69	81.45
ADAM	87.54	98.55	95.05	89.36
RMS prop	95.95	99.39	96.53	92.27

The number of images in the datasets varies among the three datasets. Therefore, the network has been trained with various epochs using the RMSprop optimiser illustrated in Fig. 7. As shown in Fig. 6, the network achieved significant results at the particular epoch. As part of network training, 80% of the data have been used for training and 20% for validation. Based on Figs. 6 and 7, the MIAS dataset achieves peak results (95.95%) with 4800 iterations for training and 160 iterations for validation with each epoch. Validation frequency and learning rates are 200 iterations and 0.0001, respectively.

The research included comparing CNN network training results with many pre-trained networks, including Alexnet, VGG-16, and VGG-19. A preprocessing step employs image transformations such as RGB conversion and prescribed image size conversion for the input images. The pre-trained networks made use of deep residual networks and simple optimisation. The weight layers in these networks are generally between 50 and 101. Table 4 describes the trail work for an epoch. Based on Table 5, these pre-trained networks produced the most accurate results with DDSM datasets. We conclude that the proposed CNN network architecture achieves optimal accuracy using these comparisons.

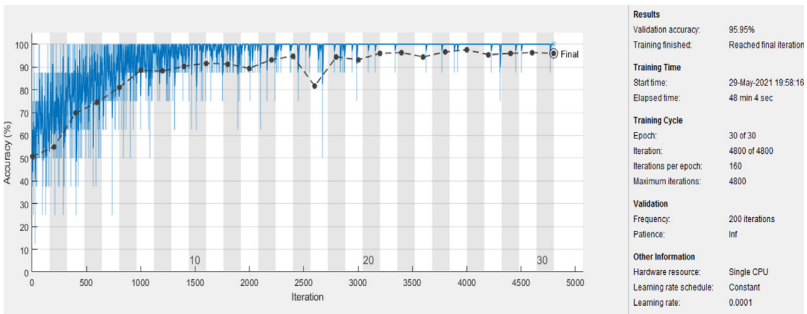

(a)

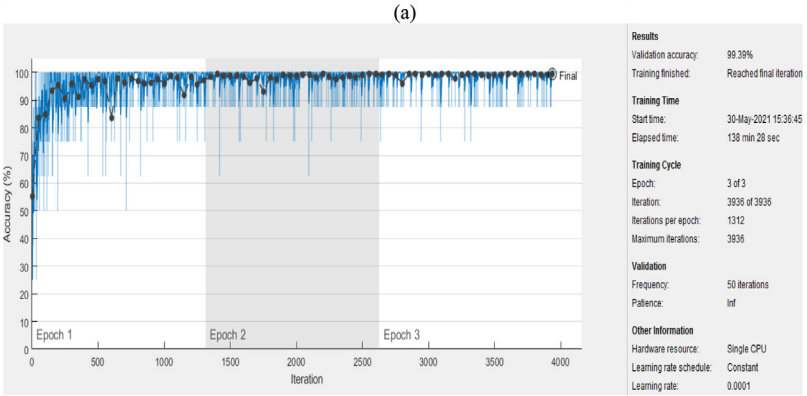

(b)

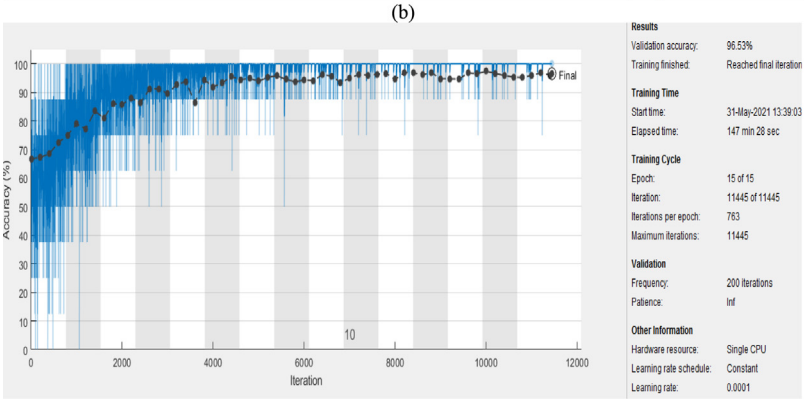

(c)

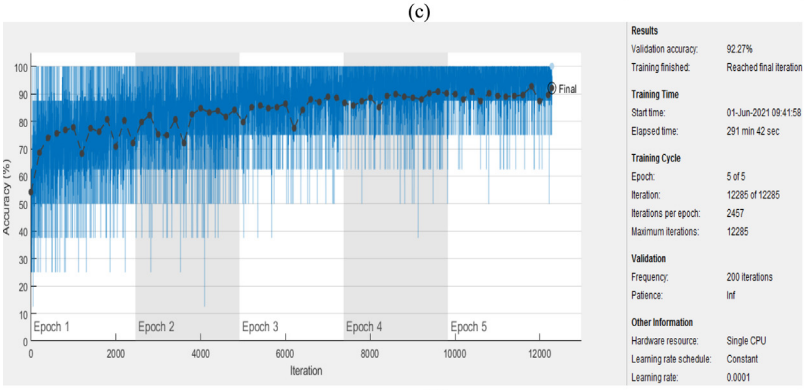

(d)

Fig. 6. Accuracy results (a) MIAS (b) DDSM (c) INbreast (d) Combined (MIAS+DDSM+INbreast).

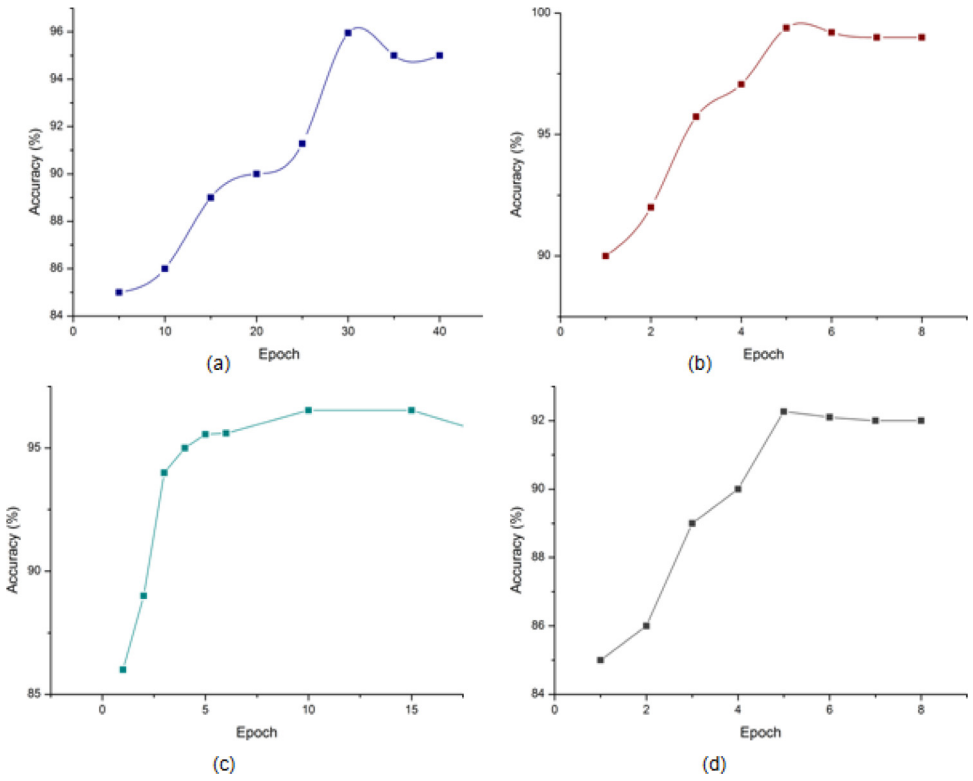

Fig. 7. Accuracies plot for different epoch using RMSprop optimizer (a) MIAS (b) DDSM (c) INbreast (d) MIAS+DDSM+INbreast.

Table 4
Accuracy analysis in Epochs.

Datsets	Accuracy (Epoch)		
MIAS	90% (20)	91.28% (25)	95.95% (30)
DDSM	95.73% (3)	97.07% (4)	99.39% (5)
INbreast	94.56% (5)	96.53% (10)	96.53% (15)
MIAS+DDSM+INbreast	85% (1)	86.33% (2)	92.27% (5)

Table 5
Comparative results analysis using pre-trained models.

Pre-trained Networks	MIAS (%)	DDSM (%)	INbreast (%)	MIAS+ DDSM+ INBREAST (%)
Alexnet	62.20	99.52	56.63	85.45
VGG-16	86.42	95.04	79.37	89.25
VGG-19	85.93	92.75	82.55	91.69

Identifying benign and malignant cases of breast cancer poses many challenges for physicians. According to this study, the model can enhance radiologists' diagnostic ability. These experiments have shown that the proposed model significantly improves existing CAD systems. Table 6 provides an overview of the literature review. In the reviewed studies, the same datasets (MIAS, DDSM, INbreast, and combined datasets) are used as in the current study. This table demonstrates that the proposed deep CNN model achieved precise accuracy using the benchmark datasets. This model will allow radiologists to acquire faultless results while minimising their workload.

Table 6
Reviewed studies comparison with the proposed approach.

Ref. No	Year	Accuracy result	Database	Method
[10]	2020	91.5% (MIAS)	MIAS	Discrete wavelet transforms and Gray Level Co-occurrence Matrix (GLCM) and Deep Belief Network (DBN).
[11]	2019	99% Bethezata General Hospital (BGH), 97.46% (MIAS)	112 — abnormal and 208 — normal (Both BGH and MIAS)	GLCM and Gabor features and one CNN based feature are evaluated with five classifiers
[12]	2020	97.9% (MIAS) and 92.61% (DDSM)	MIAS and DDSM	Wrapper-based parameter optimised kernel extreme learning machine (KELM)
[13]	2019	Support Vector Machine (SVM)-96.9%, K-nearest neighbour (KNN)-93.8, linear discriminant analysis (LDA)-89.7% and Decision T ree-88.7%	MIAS	K-means clustering and multi-class support vector machine (MSVM).
[14]	2017	CNN accuracy-87% (MIAS masses), CNN training accuracy-98% (MIAS), CNN accuracy-88% (BCDR), CNN training accuracy-98% (BCDR),	51 malignant in MIAS and 56 malignant in BCDR. (All class are distributed equally).	Deep convolution neural network
[15]	2017	94.57% (MIAS) and 85.42% (DDSM)	MIAS and DDSM	Local Binary Patterns and FLDA
[16]	2016	92.2%	MIAS	Morphological method and the random sample consensus (RANSAC) algorithm
[17]	2017	81.83% (CNN-DW) and 83.74% (CNN-CT)	MIAS	Two dimensional discrete wavelet transform (2D-DWT), Discrete curvelet transform [43] (DCT) and convolutional neural network (CNN)
[18]	2020	92.1%	MIAS	Augmented data used with CNN
[19]	2020	85.95%	7989 images of the Digital Database for Screening Mammography (DDSM)	Data augmentation and training with tests of six based U-Net models
[20]	2020	81.13% (DCNN), 89.90% (All-CNN), 90.70% (Multiscale CNN), 96.47% (MA-CNN)	MIAS	Multiscale All Convolutional Neural Network (MA-CNN)
[21]	2020	94.30%	Combined CBIS-DDSM, mini-MIAS and INbreast dataset	Features fusion with CNN
[22]	2021	96% (DDSM) and 95% (MIAS)	DDSM and MIAS	Breast Mass Classification system (BMC) — Combination of k-mean clustering, Long Short-Term Memory network of Recurrent Neural Network (RNN), CNN, random forest, boosting techniques
[23]	2020	0.8906 (Model 1) and 0.875 (Model 2)	MIAS	Deep fusion models based on VGG16 and VGG19

(*continued on next page*)

Table 6 (*continued*).

Ref. No	Year	Accuracy result	Database	Method
[26]	2021	93.39% (MIAS), 91.2% (DDSM), 93.04% (INbreast), and 90.17% (MIAS+DDSM+INbreast)	MIAS, DDSM, INbreast and MIAS+DDSM+INbreast	Deep CNN model
Proposed approach		95.95% (MIAS), 99.39% (DDSM), 96.53% (INbreast), and 92.27% (MIAS+DDSM+INbreast)	MIAS, DDSM, INbreast and MIAS+DDSM+INbreast	Deep CNN model and pre-trained network

5. Conclusion

The deep learning-based CNN screening procedure significantly improves performance over the conventional methods. Also, different hyperparameter tuning strategies are implemented to improve the classification results. Our experimental results show that the proposed method outperforms other related breast cancer classification tasks and mammography diagnosis using the benchmark datasets MIAS, INbreast, and DDSM. The obtained classification accuracy using MIAS, DDSM and INbreast datasets were 95.95%, 99.39%, and 96.53%, respectively. As evidenced by simulation results, our proposed model is significantly more impactful than other well-known models. It can therefore be applied for real-time clinical applications. The work can be extended in the future by including real-time hospital images and deeper architectures. Furthermore, different breast cancer imaging modalities will be considered for early detection.

CRediT authorship contribution statement

R. Karthiga: Conceptualization, Methodology, Software, Data curation, Visualization, Investigation, Writing – original draft. **K. Narasimhan:** Supervision, Visualization, Investigation, Data curation. **Rengarajan Amirtharajan:** Software, Validation, Writing – review & editing.

Declaration of competing interest

The authors declare that they have no known competing financial interests or personal relationships that could have appeared to influence the work reported in this paper.

Acknowledgements

Authors thank Department of Science & Technology, New Delhi, for the FIST funding (SR/FST/ET-I/2018/221(C)). Also, authors wish to thank the Intrusion Detection Lab at the School of Electrical & Electronics Engineering, SASTRA Deemed University, for providing infrastructural support to carry out this research work.

Ethical approval

This article does not contain any studies with human participants or animals performed by any authors.

References

[1] F. Bray, J. Ferlay, I. Soerjomataram, R.L. Siegel, L.A. Torre, A. Jemal, Global cancer statistics 2018: GLOBOCAN estimates of incidence and mortality worldwide for 36 cancers in 185 countries, CA Cancer J. Clin. 68 (2018) 394–424.

[2] C. Herskind, V. Steil, U. Kraus-Tiefenbacher, F. Wenz, Radiobiological aspects of intraoperative radiotherapy (IORT) with isotropic low-energy X rays for early-stage breast cancer, Radiat. Res. 163 (2005) 208–215, http://dx.doi.org/10.1667/RR3292.

[3] R.S. Lee, Francisco Gimenez, A. Hoogi, K. Miyake, Mia Gorovoy, D. Rubin, A curated mammography data set for use in computer-aided detection and diagnosis research, Sci. Data 4 (2017) 170–177, http://dx.doi.org/10.1038/sdata.2017.177.

[4] S. Saxena, M. Gyanchandani, Machine learning methods for computer-aided breast cancer diagnosis using histopathology: A narrative review, J. Med. Imaging Radiat. Sci. 51 (2020) 182–193, http://dx.doi.org/10.1016/j.jmir.2019.11.001.

[5] Mohamed Abdel-Nasser, Antonio Moreno, Mohamed A. Abdel wahab, Adel Saleh, Saddam Abdulwahab1, Vivek K. Singh, Domenech Puig, Matching tumour candidate points in multiple mammographic views for breast cancer detection, in: International Conference on Innovative Trends in Computer Engineering, ITCE, 2019, pp. 202–207.
[6] F.F. Ting, K.S. Sim, Self- regulated multilayer perceptron neural network for breast cancer classification, in: International Conference on Robotics, Automation and Sciences, ICORAS, 2017, pp. 1–5.
[7] R.M. Rangayyan, F.J. Ayres, J.E.L. Desautels, A review of computer-aided diagnosis of breast cancer: Toward the detection of subtle signs, J. Franklin Inst. 344 (2007) 312–348, http://dx.doi.org/10.1016/j.jfranklin.2006.09.003.
[8] Mohamed Meselhy Eltoukhy, Ibrahima Faye, Brahim Belhaouari Samir, A statistical based feature extraction method for breast cancer diagnosis in digital mammogram using multiresolution representation, Comput. Biol. Med. 42 (1) (2012) 123–128, http://dx.doi.org/10.1016/j.compbiomed.2011.10.016,
[9] L. Gill Naul, Jeff Hoffmeister, Improvement in sensitivity of screening mammography with computer-aided detection: a multiinstitutional trial, Am. J. Roentgenol. 181 (2003) 687–693, https://www.ajronline.org/doi/10.2214/ajr.181.3.1810687.
[10] L. Shen, M. He, N. Shen, N. Yousefi, C. Wang, G. Liu, Optimal breast tumor diagnosis using discrete wavelet transform and deep belief network based on improved sunflower optimisation method, Biomed. Signal Process. Control 60 (2020) 101953, http://dx.doi.org/10.1016/j.bspc.2020.101953.
[11] Taye Girma Debelee, Abrham Gebreselasie, Friedhelm Schwenker, Mohammadreza Amirian, Dereje Yohannes, Classification of mammograms using texture and CNN based extracted features, J. Biomim. Biomater. Biomed. Eng. 42 (2019) 79–97, http://dx.doi.org/10.4028/www.scientific.net/JBBBE.42.79.
[12] F. Mohanty, S. Rup, B. Dash, Automated diagnosis of breast cancer using parameter optimised kernel extreme learning machine, Biomed. Signal Process. Control 62 (2020) 102108, http://dx.doi.org/10.1109/access.2019.2892795.
[13] Prabhpreet Kaur, Gurvinder Singh, Parminder Kaur, Intellectual detection and validation of automated mammogram breast cancer images by multi-class SVM using deep learning classification, Inf. Med. Unlocked 16 (2019) 100151, http://dx.doi.org/10.1016/j.imu.2019.01.001.
[14] P.U. Hepsağ, S.A. Özel, A. Yazıcı, Using deep learning for mammography classification, in: 2017 International Conference on Computer Science and Engineering, UBMK, 2017, pp. 418–423, http://dx.doi.org/10.1109/UBMK.2017.8093429.
[15] R. Rabidas, A. Midya, J. Chakraborty, Neighborhood structural similarity mapping for the classification of masses in mammograms, IEEE j. biomed. health inf. 22 (2017) 826–834, http://dx.doi.org/10.1109/jbhi.2017.2715021.
[16] W.B. Yoon, J.E. Oh, E.Y. Chae, H.H. Kim, S.Y. Lee, K.G. Kim, Automatic detection of Pectoral Muscle Region for computer-aided diagnosis using MIAS mammograms, Biomed. Res. Int. (2016) 5967580, http://dx.doi.org/10.1155/2016/5967580.
[17] M.M. Jadoon, Q. Zhang, I.U. Haq, S. Butt, A. Jadoon, Three-class mammogram classification based on descriptive CNN features, Biomed. Res. Int. (2017) 3640901, http://dx.doi.org/10.1155/2017/3640901.
[18] Saleem Z. Ramadan, Using convolutional neural network with cheat sheet and data augmentation to detect breast cancer in mammograms, Comput. math. methods med. (2020) 1–9, http://dx.doi.org/10.1155/2020/9523404.
[19] F.A. Zeiser, C.A. da Costa, T. Zonta, et al., Segmentation of masses on mammograms using data augmentation and deep learning, J. Digit. Imaging 33 (2020) 858–868, http://dx.doi.org/10.1007/s10278-020-00330-4.
[20] S.A. Agnes, J. Anitha, S.I.A. Pandian, J.D. Peter, Classification of mammogram images using multiscale all convolutional neural network (MA-CNN), J. Med. Syst. 44 (2019) http://dx.doi.org/10.1007/S10916-019-1494-Z.
[21] Qian Zhang, Yamei Li, Guohua Zhao, Panpan Man, Yusong Lin, Meiyun Wang, A novel algorithm for breast mass classification in digital mammography based on feature fusion, J. Healthcare Eng. (2020) http://dx.doi.org/10.1155/2020/8860011.
[22] S.J. Malebary, A. Hashmi, Automated breast mass classification system using deep learning and ensemble learning in digital mammogram, IEEE Access 9 (2021) 55312–55328, http://dx.doi.org/10.1109/ACCESS.2021.3071297.
[23] X. Yu, W. Pang, Q. Xu, M. Liang, Mammographic image classification with deep fusion learning, Sci. Rep. 10 (2020) 14361.
[24] N. Dhungel, G. Carneiro, A.P. Bradley, A deep learning approach for the analysis of masses in mammograms with minimal user intervention, Med. image anal. 37 (2017) 114–128, http://dx.doi.org/10.1016/j.media.2017.01.009.
[25] D. Ribli, A. Horváth, Z. Unger, P. Pollner, I. Csabai, Detecting and classifying lesions in mammograms with deep learning, Sci. rep. 8 (2018) 1–7.
[26] Enas M.F. El Houby, Nisreen I.R. Yassin, Malignant and nonmalignant classification of breast lesions in mammograms using convolutional neural networks, Biomed. Signal Process. Control 70 (2021) 102954, http://dx.doi.org/10.1016/j.bspc.2021.102954.
[27] J. Suckling, J. Parker, D. Dance, S. Astley, I. Hutt, C. Boggis, I. Ricketts, et al., Mammographic Image Analysis Society (MIAS) database v1.21, https://www.repository.cam.ac.uk/handle/1810/250394.
[28] M. Heath, K. Bowyer, D. Kopans, R. Moore, W.P. Kegelmeyer, The digital database for screening mammography, in: Proceedings of the 5th International Workshop on Digital Mammography, Medical physis Publishing, 2000, pp. 212–218, ISBN 1-930524-00-5.
[29] C. Moreira, I. Amaral, I. Domingues, A. Cardoso, M.J. Cardoso, J.S. Cardoso, Inbreast: toward a full-field digital mammographic database, Acad. Radiol. 19 (2012) 236–248.
[30] Ting Lin, Mei-Ling Huang, Dataset of breast mammography images with masses, Mendeley Data V2 (2020) http://dx.doi.org/10.1007/s10278-020-00330-4.
[31] S. Don, D. Min, Breast skin line segmentation on digital mammogram using fractal approach, Indian J. Sci. Technol. 9 (2016) 1–7, http://dx.doi.org/10.17485/ijst/2016/v9i31/85420.
[32] J.C.M. dos Santos, G.A. Carrijo, others de Fátima dos Santos Cardoso, Fundus image quality enhancement for blood vessel detection via a neural network using CLAHE and Wiener filter, Res. Biomed. Eng. 36 (2020) 107–119, http://dx.doi.org/10.1007/s42600-020-00046-y.
[33] Soumen Biswas, Dibyendu Ghoshal, Ranjay Hazra, A new algorithm of image segmentation using curve fitting based higher order polynomial smoothing, Optik 127 (2016) 8916–8925, http://dx.doi.org/10.1016/J.IJLEO.2016.06.110.

[34] M.B. Morgan, J.L. Mates, Applications of artificial intelligence in breast imaging, Radiol. Clin. North Am. 59 (1) (2021) 139–148, http://dx.doi.org/10.1016/j.rcl.2020.08.007, PMID: 33222996.
[35] K.J. Geras, R.M. Mann, L. Moy, Artificial intelligence for mammography and digital breast tomosyn thesis: Current concepts and future perspectives, Radiology 293 (2) (2019) 246–259, http://dx.doi.org/10.1148/radiol.2019182627, Epub 2019 Sep 24. PMID: 31549948; PMCID: PMC6822772.
[36] I. Hoshino, H. Yokota, Radiogenomics of gastroenterological cancer: The dawn of personalised medicine with artificial intelligence-based image analysis, Ann. Gastroenterol. Surg. 5 (4) (2021) 427–435, http://dx.doi.org/10.1002/ags3.12437, PMID: 34337291; PMCID: PMC8316732.
[37] A. Bitencourt, Naranjo I. Daimiel, R. Lo Gullo, C. Rossi Saccarelli, Pinker. K., AI-enhancedbreast imaging: Where are we and where are we heading?, Eur. J. Radiol. 142 (2021) 109882, http://dx.doi.org/10.1016/j.ejrad.2021.109882, Epub 2021 Jul 30. PMID: 34392105; PMCID: PMC8387447.
[38] G. Huang, Z. Liu, L. Van Der Maaten, K.Q. Weinberger, Densely connected convolutional networks, in: CVPR, vol. 1, 2017, https://arxiv.org/abs/1608.06993v5.
[39] R. Cichy, A. Khosla, D. Pantazis, A. Torralba, A. Oliva, Mapping human visual representations in space and time by neural networks, J. Vis. 15 (2015) http://dx.doi.org/10.1167/15.12.376.
[40] B. Zhou, A. Lapedriza, J. Xiao A. Torralba, A. Oliva, Learning deep features for scene recognition using places database, Adv. neural inf. process. syst. (2014) 487–495, https://dl.acm.org/doi/10.5555/2968826.2968881.
[41] A. Krizhevsky, I. Sutskever, G.E. Hinton, Imagenet classification with deep convolutional neural networks, Commun. ACM 60 (2017) 84–90, http://dx.doi.org/10.1145/3065386[10.1145/3065386.
[42] O. Russakovsky, J. Deng, H. Su, et al., ImageNet large scale visual recognition challenge, Int. J. Comput. Vis. 115 (2015) 211–252, http://dx.doi.org/10.1007/s11263-015-0816-y.
[43] R. Karthiga, K. Narasimhan, Medical imaging technique using curvelet transform and machine learning for the automated diagnosis of breast cancer from thermal image, Pattern Anal. Appl. 24 (2021) 981–991, http://dx.doi.org/10.1007/s10044-021-00963-3.